Single-Electron Force Readout of Nanoparticle Electrometers Attached to Carbon Nanotubes

Jun Zhu,[*,†,‡,§] **Markus Brink,**[†,§,⊥] **and Paul L. McEuen**[†]

*Laboratory of Atomic and Solid State Physics, Cornell University,
Ithaca, New York 14853, and Department of Physics, Penn State University,
University Park, Pennsylvania 16802*

ABSTRACT

We introduce a new technique of probing the local potential inside a nanostructure employing Au nanoparticles as electrometers and using single-electron force microscopy to sense the charge states of the Au electrometers, which are sensitive to local potential variations. The Au nanoelectrometers are weakly coupled to a carbon nanotube through high-impedance molecular junctions. We demonstrate the operation of the Au nanoelectrometer, determine the impedance of the molecular junctions, and measure the local potential profile in a looped nanotube.

The local potential inside a conductor becomes increasingly challenging to obtain as the dimensions of modern devices shrink into the nano regime. New methods need to be developed to reduce the size of voltage probes and control their placement and coupling to the device under examination. In addition, the perturbation of the measurement on the device itself cannot be neglected and must be assessed. In recent years, several innovative approaches have been put forward to address these challenges. These include, for example, the usage of a conducting atomic force microscope (AFM) tip as a sliding electrode[1–3] or in electrostatic force microscopy,[4] on-site quantum point contacts[5] and single electron transistors (SETs)[6] with high voltage sensitivities, and scanned SETs[7] which are mobile and sensitive. In this report, we present a new scheme that combines locally placed Au nanoparticles with AFM-based single-electron force sensing microscopy to function as weakly perturbative, highly sensitive nanoelectrometers. The Au nanoelectrometer senses the local electrostatic potential via its single-electron charge states. Its large input impedance, produced by a molecular junction and measured by dissipation force microscopy, ensures weak coupling to the device. We demonstrate the operation of the Au nanoelectrometers by mapping the local potential profile of a looped carbon nanotube (CNT). This new type of nanoparticle-based electrometer can be generalized to map potential distributions in other nanostructures such as nanowires and two-dimensional (2D) conductors. The impedance measurement can be used to probe the resistance of molecular junctions.

The Au nanoparticle (mean diameter 12 nm) electrometers are integrated into a CNT field effect transistor[8] via chemical linkers (see Supporting Information for details). A schematic of the CNT-Au assembly is shown in Figure 1a. The linker molecule consists of a pyrene ($C_{16}H_{10}$) end group, a backbone of amide-containing alkyl chain $(CH_2)_3-CO-NH-(CH_2)_2$ of approximately 0.8 nm in length and a thiol (SH) end group (Figure 1a). Pyrene is known to adhere to CNTs via π-orbital stacking, a weak van der Waals bond,[9] while the thiol forms a strong covalent bond with Au. An AFM image of a typical section of the CNT device is given in Figure 2a. Au nanoparticles preferentially adhere to the CNT rather than the SiO_2 substrate. Comparison experiments show that without the linker molecule, Au nanoparticles do not adhere to CNTs. The $I(V_g)$ curve of a CNT remains nearly unchanged before and after Au nanoparticle attachment, indicating that Au nanoparticles are not strong scattering centers (see Supporting Information for details).

Due to their small size and weak coupling to the nanotube, the nanoparticles exhibit single-electron charging behavior[10] at 77 K. The charge state of an Au nanoparticle is set by nearby electrostatic potentials, which is the principle behind its application as a local electrometer. The linker molecules form tunnel barriers between the CNT and the Au nanoparticles; this sets the input impedance of the nanoparticle electrometer.

We detect charge tunneling on/off the nanoparticle with the AFM cantilever.[11–13] The biased AFM tip oscillates at a

---
* Corresponding author. E-mail: jzhu@phys.psu.edu.
† Cornell University.
‡ Penn State University.
§ These authors contributed equally to this work.
⊥ Present address: Department of Applied Physics, Yale University, New Haven, Connecticut 06520.
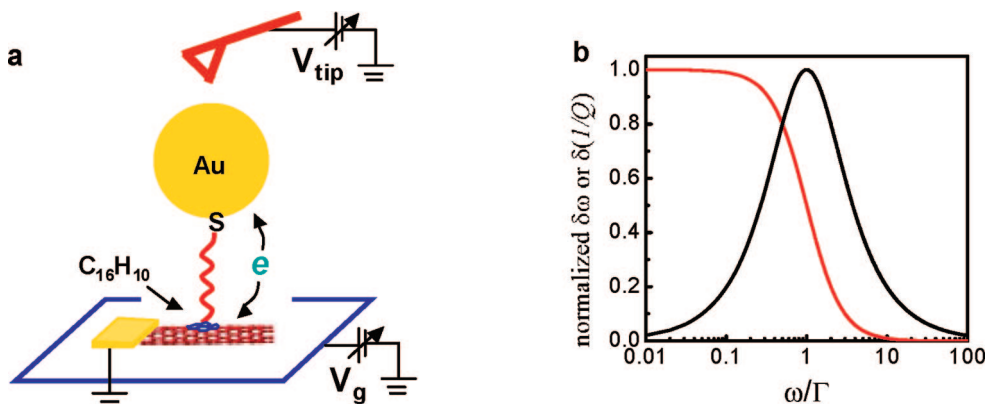
Figure 1. Schematic of our CNT-Au nanoparticle assembly and calculated response of the cantilever. (a) A schematic of our device and the gating scheme. A Au nanoparticle is linked to the CNT via a linker molecule. The backbone of the linker molecule is an amide-containing alkyl chain $-(CH_2)_3-CO-NH-(CH_2)_2-$. The Au particle is gated by the AFM tip, the CNT, and the silicon n^{++} global backgate. The CNT is contacted by two Au electrodes (one shown). (b) Theoretical behavior of the frequency shift ($\delta\omega$) and dissipation ($\delta(1/Q)$) signal of the AFM cantilever as a function of ω/Γ. Both are normalized by their maximum values. $\delta\omega$ (red line) decreases monotonically with increasing ω/Γ while $\delta(1/Q)$ (black line) maximizes at $\omega/\Gamma = 1$, corresponding to $\Gamma = 9.1 \times 10^5$ s^{-1} in our setup.

height z with a small amplitude dz, imposing a perturbative ac gating effect on the Au nanoparticle. This ac gating effect induces charge transfer between the CNT and the Au, which in turn exerts an electrostatic force on the AFM cantilever and affects its motion. This noncontact force detection only requires one electrical connection to the nanoparticle (the molecular junction between the CNT and the Au nanoparticle), greatly simplifying its use as a local electrometer.

The force exerted on the AFM cantilever by tunneling charges is given by[14]

$$F_e = -\delta k \, dz \frac{1 + i\omega/\Gamma}{1 + (\omega/\Gamma)^2}$$

where

$$\delta k = \left(\frac{dq_c}{dz}\frac{e}{C_{Au}}\right)^2 f'(\Delta\varepsilon_{dc}) \qquad (1)$$

C_{Au} is the total capacitance of the Au nanoparticle; q_c is the control charge, and $f'(\Delta\varepsilon_{dc})$ is the Fermi distribution derivative as a function of the electrochemical potential misalignment between the CNT and the Au nanoparticle. Since charges tunnel across the barrier between the CNT and the Au nanoparticle at a finite rate Γ, a phase lag develops between the motion of the AFM tip and the induced charge motion. The real component of the force in eq 1 corresponds to a Coulomb-softening of the cantilever's spring constant and a decrease in the resonance frequency by $\delta\omega$, and the imaginary component causes additional damping, which can be expressed as a degradation of the cantilever's quality factor Q:

$$\frac{\delta\omega}{\omega} = \frac{\delta k}{2k}\frac{1}{1 + (\omega/\Gamma)^2} \quad \delta(1/Q) = -\frac{\delta k}{k}\frac{\omega/\Gamma}{1 + (\omega/\Gamma)^2}$$

$$\omega/\Gamma = -\frac{\delta(1/Q)}{2\delta\omega/\omega} \qquad (2)$$

These two quantities, $\delta(\omega)$ and $\delta(1/Q)$, can be directly measured experimentally to yield the charge addition spectra and tunneling rates Γ on/off the nanoparticle electrometer. The former is used to measure local electrostatic potentials,

and the latter corresponds to the resistive input impedance of the electrometer, that is, the tunnel resistance of the molecular junction $R_T = 2k_BT/e^2\Gamma$.[10,14] The ω/Γ dependence of $\delta\omega$ and $\delta(1/Q)$ (eq 2) is plotted in Figure 1b. As ω/Γ increases, that is, as the tunnel barrier becomes more opaque, the frequency shift signal $\delta\omega$ monotonically decreases to zero, whereas the dissipation signal $\delta(1/Q)$ maximizes at $\omega/\Gamma = 1$. The physical meaning of the plot is clear: In the limit of a transparent barrier, the induced charges tunnel fast and in phase with the driving AFM tip. This process produces maximum frequency shift and zero dissipation. When the barrier becomes extremely opaque, charges cannot tunnel across the barrier fast enough to respond to the driving of the AFM tip, producing neither frequency shift nor dissipation. Maximum dissipation occurs when charges tunnel on the time scale of one cantilever oscillation cycle.

To measure $\delta\omega$ and $\delta(1/Q)$, we drive the AFM cantilever on resonance with a constant force amplitude F_{ext} and use a phase locked loop (PLL) circuit to monitor the resonant frequency ω (or $f = \omega/2\pi$) and oscillation amplitude dz of the cantilever. The latter directly yields the quality factor using the relation $Q = k \, dz/F_{ext}$. All measurements are carried out in a home-built AFM system operating at 77 K (see Supporting Information and refs 9–12 for details). Figure 2b shows a series of spatial scans of the AFM tip above the CNT device, with the oscillation amplitude of the cantilever plotted in color scale. We find many sets of dark, concentric rings centered at specific locations along the CNT. On the dark rings, the cantilever amplitude is generally decreased 10−20%, corresponding to an increase in dissipation, with exceptionally dark spots reaching 50%. Figure 2c gives a close-up of one Au nanoparticle. Several concentric rings are clearly visible.

A given set of rings corresponds to Coulomb oscillations of the Au nanoparticle enclosed at the center. At the position of a dark ring, the oscillating, biased AFM tip causes an electron to tunnel on and off the nanoparticle during a cantilever oscillation, producing additional electromechanical
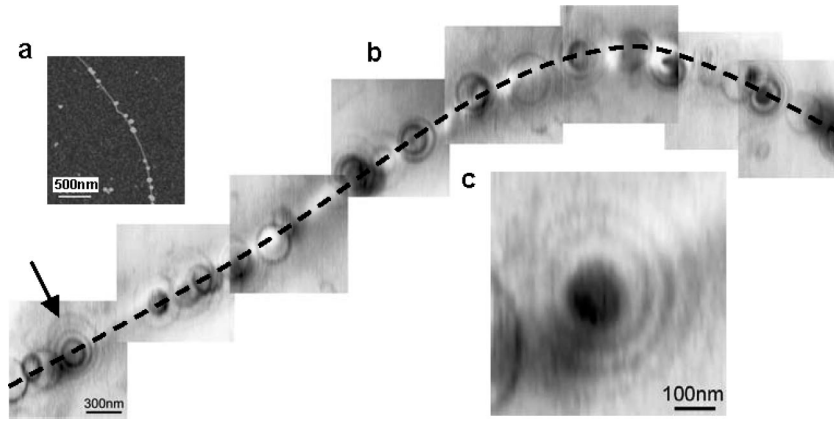
Figure 2. Coulomb oscillation behavior of Au nanoparticles. (a) Topographic AFM image of a section of the CNT device, showing selective attachment of Au nanoparticles. The CNT diameter is 3.2 nm. (b) A series of scans above the CNT device with the oscillation amplitude of the cantilever plotted in gray scale. Coulomb oscillations of the Au nanoparticles appear as concentric, dark rings centered on individual particles. Charge motion causes additional damping to the oscillation of the cantilever in the tunneling regime of the Au particles, producing a general decrease of 10−20% in oscillation amplitude with extremely dark spots reaching 50%. Black dashed line indicates the location of the CNT. All images are taken with $V_{tip} = 3$ V, $V_g = -2$ V, and tip height $z = 60$ nm. (c) A close-up image of the Au nanoparticle indicated by the arrow in b. Several concentric rings are clearly visible. Image taken with $V_{tip} = 3$ V, $V_g = -1.5$ V, and tip height $z = 60$ nm.

damping of the cantilever.[12] Between the dark rings, the nanoparticle is in Coulomb blockade, and no tunneling occurs. Nanoparticles lying on the SiO$_2$ substrate away from any electrode do not produce any signal, demonstrating the importance of the electrical connection between the CNT and the nanoparticle.

To characterize the behavior of a given nanoparticle electrometer, we vary the gating potentials V_g and V_{tip} with the tip positioned at a constant height z above the nanoparticle. Three V_g-dependent charge addition spectra of particle No. 1 taken at different V_{tip}'s are given in Figure 3. Each spectrum features periodic dips riding on a smooth background. Similar to the rings in Figure 2, each dip here corresponds to where the charge state of the nanoparticle changes. Note that the small cross section of the CNT allows the n^{++} backgate potential V_g to efficiently gate the Au nanoparticle and add charges one by one.

The average spacing between adjacent charge states is $\Delta V_g = 0.48$ V and is independent of V_{tip}. This yields the capacitance between the Au nanoparticle and the global backgate: $C_g = e/\Delta V_g = 0.33$ aF, where we have neglected the single-particle energy level spacing of the nanoparticle. The capacitance between the AFM tip and the particle C_{tip} is determined by tracking the shift of a charge state along the V_g axis as V_{tip} changes:

$$C_{tip} = C_g(\Delta V_g/\Delta V_{tip}) = 0.18 \text{ aF}$$

To determine the charging energy of the nanoparticle, we use the thermal broadening of the Coulomb oscillation peaks. If the oscillation amplitude dz of the cantilever is small, the full width at half maximum (FWHM) of a charging dip measured as a function of V_g is given by $\sim 4k_BTC_{Au}/(eC_g)$.[10] For this particle, we find $C_{Au} = (1.5 \pm 0.1)$ aF, and a charging energy $E_c = e^2/C_{Au} = (110 \pm 10)$ meV. Finally, the capacitance between the CNT and the Au is estimated to be $C_{cnt} = C_{Au} - C_{tip} - C_g = 0.99$ aF, where we have neglected any interparticle coupling and coupling to metal electrodes.
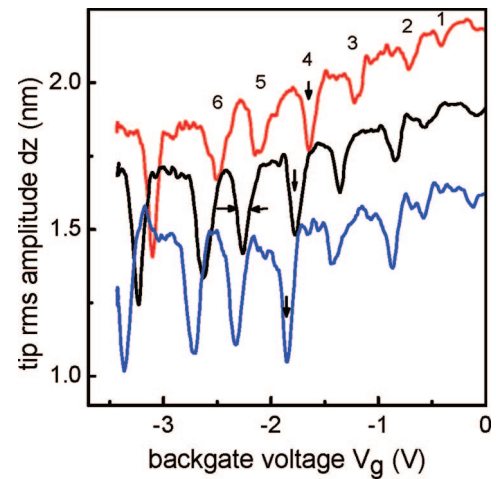

Figure 3. V_g-dependent charge addition spectra of particle No. 1. Traces correspond to $V_{tip} = 1$ V (red), 1.25 V (black), and 1.5 V (blue) respectively. Black and blue traces are shifted down vertically for clarity. Tip height $z = 60$ nm. The backgate capacitance C_g is determined by the average spacing in V_g between adjacent charge states. C_{tip} is determined by tracking the shift of a specific charge state in V_g as V_{tip} varies. Vertical arrows point to charge state #4. The total capacitance C_{Au} is extracted from the fwhm of a charging dip as indicated by the horizontal arrows. Averaging charge state 1−6 of the $V_{tip} = 1.25$ V trace, we find fwhm = (0.12 ± 0.01) V for this Au particle.

Similar measurements are repeated on several Au nanoparticles and summarized in Table 1.

Experimental values of E_c are in good agreement with theoretical estimates and FEMLAB simulations (see Supporting Information for details) based on the mean size and variation of the Au nanoparticle diameters (12 ± 2 nm). This agreement, together with the uniformity displayed by C_g and C_{tip} from different Au particles, demonstrates the reproducibility of these Au nanoparticle electrometers.

Next, we combine measurements of $\delta\omega$ and $\delta(1/Q)$ to determine Γ, the charge tunneling rate on/off the nanoparticle,

Table 1. Charging Energy and Capacitances of Au Nanoparticles

Au #	C_g (aF)	C_{tip} (aF)	C_{Au} (aF)	E_c (meV)
1	0.33	0.18	1.5	110
2	0.39	0.23	1.7	95
3	0.39	0.22	1.5	105
4	0.46	0.23	2.1	80
5	0.46	0.23	<2.1	>80
6	0.46	0.25		

and calculate the input impedance of the Au nanoparticle electrometer $R_T = 2k_B T/e^2\Gamma$. We first establish that the oscillation amplitude dz of the cantilever can be used to measure the loss rate $1/Q$, as shown in Figure 4a. In Figure 4b, we simultaneously plot frequency ω and amplitude dz of the AFM cantilever for six charge states of particle No. 1. Both signals show concurrent dips in the charge tunneling regime of the Au particle. We determine $\delta\omega$ and $\delta(1/Q)$ and calculate ω/Γ using eq 2. Variations among different charge states yield $0.32 < \omega/\Gamma < 0.78$, corresponding to a tunneling rate $\Gamma = 0.49 \times 10^6$ s^{-1} to 1.20×10^6 s^{-1} on/off the Au particle and R_T in the range of $68-166$ GΩ.

We have performed similar measurements and analyses on 12 Au nanoparticles. The average value of ω/Γ for each particle is listed: 0.13, 0.15, 0.29, 0.30, 0.32, 0.39, 0.50, 0.50, 0.55, 0.61, 0.65, 0.66. They correspond to $\Gamma = 5.8 \times 10^5$ s^{-1} to 3×10^6 s^{-1} or 27 GΩ < R_T < 140 GΩ. The large values of R_T help ensure weak coupling, and hence weak perturbation of our Au nanoelectrometers to the CNT.

The impedance of the electrometer is determined by the junction between the CNT and the nanoparticle. On the basis of data in the literature[15](see Supporting Information for details), the tunnel resistance of the alkyl chain is estimated to be ~300 MΩ. By adding resistances due to the tunnel barrier between the CNT and the pyrene and the partial orbital overlap between the pyrene molecule and the alkyl chain, R_T in the range of our measurements is reasonable. The approximate 5-fold variation in R_T is not surprising given the expected variability in the number of linker molecules attached to each Au particle and the different conformational states of the linker molecule and the Au–S bonding sites.[16,17] Surprisingly, variability is also seen in tunneling rates for the different charge states of the same nanoparticle (see, e.g. Figure 4). While the origin of this behavior is not known, electrostatic interactions with neighboring Au nanoparticles or with charged impurities may be responsible.

Having demonstrated the operation of the nanoparticle electrometers, we now use them to probe the local potential in a CNT circuit. In particular, we apply a dc bias to establish a current flow in the CNT and measure the local voltage drop in the looped, 35 μm long CNT shown in Figure 5a. This measurement provides a straightforward way of resolving the important issue of whether significant tunneling occurs at the crossover point of the loop.[18–20]

The idea is as follows: similar to a change in V_g, a potential change in the CNT shifts the charge state of a bound nanoparticle. Once calibrated, this shift provides a means of measuring the local potential within the device. This procedure is illustrated in Figure 5b. Shown is one Coulomb
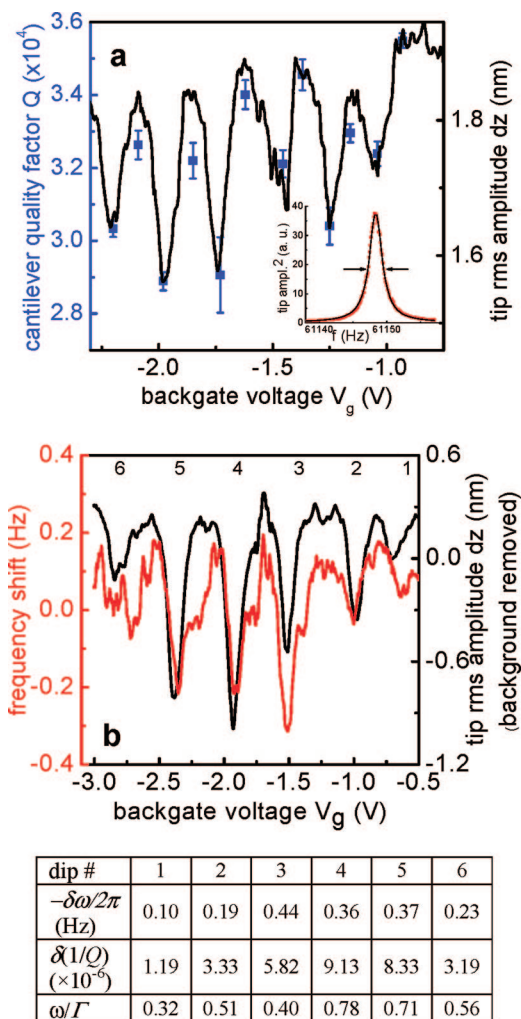

dip #	1	2	3	4	5	6
$-\delta\omega/2\pi$ (Hz)	0.10	0.19	0.44	0.36	0.37	0.23
$\delta(1/Q)$ ($\times 10^{-6}$)	1.19	3.33	5.82	9.13	8.33	3.19
ω/Γ	0.32	0.51	0.40	0.78	0.71	0.56

Figure 4. Determining charge tunneling rate Γ on/off a Au nanoparticle with frequency shift and dissipation microscopy. (a) Linear scaling between the quality factor Q (blue squares) and the oscillation amplitude dz (black trace) of the AFM cantilever. Q is extracted from the FWHM of a cantilever's resonance curve in frequency domain. Inset: A typical resonance curve of the cantilever. (b) Frequency (red trace) and amplitude (black trace) of the AFM cantilever measured simultaneously while sweeping V_g. Both signals show concurrent dips in the open regime of the Au nanoparticle. $V_{tip} = 1$ V, tip height $z = 60$ nm. Smoothly varying background is removed in both traces. Values of $\delta\omega$, $\delta(1/Q)$, and the resulting ω/Γ for the six charging dips marked in (b) are given in the table below. $0.32 < \omega/\Gamma < 0.78$ corresponds to tunneling rate 0.49×10^6 s$^{-1} < \Gamma < 1.20 \times 10^6$ s^{-1}. Figure table: Frequency shift and Q-degradation signal from single-electron charging of a Au nanoparticle.

oscillation for a particular nanoparticle at four different configurations of the electrode potentials: (A) $V_l = V_r = 0$ V (B) $V_l = 0.2$ V, $V_r = 0$ V, (C) $V_l = 0$ V, $V_r = 0.2$ V, (D) $V_l = V_r = 0.2$ V, where V_l and V_r are potentials applied to the left and right electrode, respectively. Configurations A and D allow us to calibrate the shift of the CNT's electrochemical potential (see Supporting Information for details), which is then used to read the local potential of the CNT under forward (B) and reverse (C) bias. The voltage resolution of the set up is ± 3 mV and can be further improved by lowering the measurement temperature and/or reducing the noise level. Normalized potential readings from
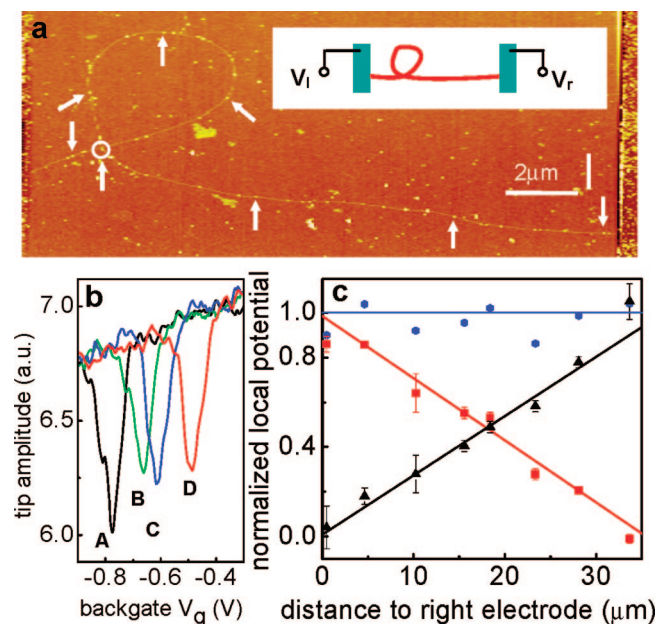
Figure 5. Potential profile of a looped CNT device measured with local Au nanoparticle voltmeters. (a) Topographic AFM image of the CNT device. The CNT diameter is 2.4 nm. Arrows point to Au particles selected as voltmeters. Inset illustrates the measurement scheme. (b) The shift of a charge state in 4 electrode configurations: (A) $V_l = V_r = 0$ V (B) $V_l = 0.2$ V, $V_r = 0$ V (C) $V_l = 0$ V, $V_r = 0.2$ V (D) $V_l = V_r = 0.2$ V (data from the circled Au particle in (a)). (c) Normalized local potential of the CNT in forward ((B), black triangles) and reverse ((C), red squares) bias. The sum of the two gives unity (blue circles). The linear potential profile along the whole length of the CNT indicates diffusive transport. The precise resistance of the looped NT is unknown because of another NT in parallel (not shown). $R_{total} \sim 120$ kΩ in the V_g range used in this manuscript, consistent with other NTs grown and fabricated in the same batch (8 total).

8 Au nanoparticles along the length of the looped nanotube are plotted in Figure 5c. The potential drop in the CNT exhibits a linear profile along the whole length, including the loop. We conclude that direct tunneling at the loop crossing point is not important in our device and that the current flows predominantly around the loop. The linear voltage drop also indicates that transport is diffusive through this long CNT device. This observation is consistent with other reports in the literature, where the mean free path of a CNT is found to range from hundreds of nanometers to a few micrometers.[21-23] Also, since there is no significant potential drop at the metallic electrodes, the contact resistance is negligible in comparison to the resistance of the CNT itself.

The nanoparticle electrometer scheme presented here has a number of advantages in comparison with other techniques to measure local potentials. Unlike contact-probe AFM,[1-3] the Au nanoparticle electrometers are mechanically non-invasive. Compared with electrostatic force microscopy,[4] the single electron transistor-based readout method has higher sensitivity and does not need background removal. Unlike scanned SETs,[7] the fabrication and integration of the Au nanoelectrometers into devices are relatively easy. Our force sensing techniques demonstrated at 77 K could potentially operate at room temperature, leading to wide usage of this method.

In conclusion, we have demonstrated the fabrication, characterization, and operation of Au nanoparticle electrometers on CNTs using AFM-based force sensing techniques. The commercial availability of AFM cantilevers of a range of resonant frequencies, Au nanoparticles of different sizes, and linker molecules of varying impedances expands the measurement range and applicability of this technique. By using suitable linker chemistries, it should be straightforward to implement the approach we described here to other material systems such as Si nanowires[24] and graphene. Additionally, the impedance measurement provides a novel method to determine the resistance of single or few molecular junctions. The fabrication process is significantly simplified since only one electrical contact to the nanoparticle is required. The molecules themselves need not form an ordered monolayer or bridge electrodes separated by ~1 nm gap.[25] This dissipation force technique is an important new tool that complements existing transport-based methods to study molecular conductors.

Supporting Information Available: Methods on Au nanoparticle synthesis, linker molecule synthesis, Au nanoparticle attachment. Parameters of the AFM cantilever. FEMLAB simulations of the capacitances of the system. Estimation of the tunneling current and power dissipation in Au nanoparticle charging events. Estimation of the alkyl chain resistance. Calibration of the Au nanoparticle nanoelectrometer. Additional data and discussions on the perturbative effects of the technique. This material is available free of charge via the Internet at http://pubs.acs.org.

References

(1) Dai, H.; Wong, E. W.; Lieber, C. M. *Science* **1996**, *272* (5261), 523–526.
(2) Yaish, Y.; Park, J. Y.; Rosenblatt, S.; Sazonova, V.; Brink, M.; McEuen, P. L. *Phys. Rev. Lett.* **2004**, *92* (4), 046401.
(3) Gomez-Navarro, C.; de Pablo, P. J.; Gomez-Herrero, J. *J. Mater. Sci.-Materials in Electronics* **2006**, *17* (6), 475–482.
(4) Bachtold, A.; Fuhrer, M. S.; Plyasunov, S.; Forero, M.; Anderson, E. H.; Zettl, A.; McEuen, P. L. *Phys. Rev. Lett.* **2000**, *84* (26), 6082–6085.
(5) Elzerman, J. M.; Hanson, R.; Greidanus, J. S.; van Beveren, L. H. W.; De Franceschi, S.; Vandersypen, L. M. K.; Tarucha, S.; Kouwenhoven, L. P. *Phys. Rev. B* **2003**, *67* (16), 161308.
(6) Ilani, S.; Yacoby, A.; Mahalu, D.; Shtrikman, H. *Phys. Rev. Lett.* **2000**, *84* (14), 3133.
(7) Yoo, M. J.; Fulton, T. A.; Hess, H. F.; Willett, R. L.; Dunkleberger, L. N.; Chichester, R. J.; Pfeiffer, L. N.; West, K. W. *Science* **1997**, *276* (5312), 579–582.
(8) McEuen, P. L.; Fuhrer, M. S.; Park, H. K. *IEEE Transactions on Nanotechnology* **2002**, *1* (1), 78–85.
(9) Chen, R. J.; Zhang, Y. G.; Wang, D. W.; Dai, H. J. *J. Am. Chem. Soc.* **2001**, *123* (16), 3838–3839.

(10) Grabert, H.; Devoret, M. H. *Single charge tunneling: Coulomb blockade phenomena in nanostructures*; Plenum Press: New York, 1992; Vol. 294.

(11) Woodside, M. T. *Scanned Probe Microscopy of the Electronic Properties of Low-Dimensional Systems.* Ph. D. Thesis, University of California, Berkeley, 2001.

(12) Woodside, M. T.; McEuen, P. L. *Science* **2002**, *296* (5570), 1098–1101.

(13) Zhu, J.; Brink, M.; McEuen, P. L. *Appl. Phys. Lett.* **2005**, *87* (24), 242102.

(14) Brink, M. *Imaging single-electron charging in nanostructures by low-temperature scanning force microscopy.* Ph. D. Thesis, Cornell University, 2006.

(15) Monnell, J. D.; Stapleton, J. J.; Dirk, S. M.; Reinerth, W. A.; Tour, J. M.; Allara, D. L.; Weiss, P. S. *J. Phys. Chem. B* **2005**, *109* (43), 20343–20349.

(16) Venkataraman, L.; Klare, J. E.; Nuckolls, C.; Hybertsen, M. S.; Steigerwald, M. L. *Nature* **2006**, *442* (7105), 904–907.

(17) Nitzan, A.; Ratner, M. A. *Science* **2003**, *300* (5624), 1384–1389.

(18) Fuhrer, M. S.; Nygard, J.; Shih, L.; Forero, M.; Yoon, Y. G.; Mazzoni, M. S. C.; Choi, H. J.; Ihm, J.; Louie, S. G.; Zettl, A.; McEuen, P. L. *Science* **2000**, *288* (5465), 494–497.

(19) Refael, G.; Heo, J.; Bockrath, M. *Phys. Rev. Lett.* **2007**, *98* (24), 246803–4.

(20) Freitag, M.; Tsang, J. C.; Kirtley, J.; Carlsen, A.; Chen, J.; Troeman, A.; Hilgenkamp, H.; Avouris, P. *Nano Lett.* **2006**, *6* (7), 1425–1433.

(21) Javey, A.; Guo, J.; Paulsson, M.; Wang, Q.; Mann, D.; Lundstrom, M.; Dai, H. J. *Phys. Rev. Lett.* **2004**, *92* (10), 106804.

(22) Park, J. Y.; Rosenblatt, S.; Yaish, Y.; Sazonova, V.; Ustunel, H.; Braig, S.; Arias, T. A.; Brouwer, P. W.; McEuen, P. L. *Nano Lett.* **2004**, *4* (3), 517–520.

(23) Zhou, X. J.; Park, J. Y.; Huang, S. M.; Liu, J.; McEuen, P. L. *Phys. Rev. Lett.* **2005**, *95* (14), 146805.

(24) Bent, S. F. *Surf. Sci.* **2002**, *500* (1−3), 879–903.

(25) Selzer, Y.; Allara, D. L. *Annu. Rev. Phys. Chem.* **2006**, *57*, 593–623.

NL801295Y